Phase symmetry analysis for nonlinear ultrasonic modulated signals

[1]Gian-Piero Malfense Fierro, [2]Francesco Ciampa, [1]Michele Meo

[1]Department of Mechanical Engineering, University of Bath, Bath, BA2 7AY, UK

[2]Department of Mechanical Engineering Sciences, University of Surrey, Guildford, GU2 7XH, UK

Abstract

Nonlinear ultrasonic experiments typically require digital pass-band filters and advanced signal processing tools to highlight low-amplitude nonlinear elastic effects such as harmonics, sub-harmonics and sidebands, which are used as signatures for the presence of damage. However, current signal processing techniques cannot be used with dual periodic excitation without reducing signal frequency resolution and severely altering measured waveforms. This paper reports the theoretical development of phase symmetry analysis for nonlinear ultrasound with dual periodic transmission. The proposed signal post-processing technique consists of determining the phase angles of transmitted waveforms that allow filtering modulated nonlinear ultrasonic waves from the measured signal spectrum. Experimental results validated theoretical predictions and revealed that phase symmetry analysis method provides an easy-to-implement and reliable procedure to extract sidebands from the measured signal noise. Phase symmetry analysis with dual excitation has, therefore, the potential to enable sensitive and efficient nonlinear ultrasound testing for various materials, damage scenarios and applications.

1. Introduction

Non-destructive testing and evaluation (NDT/E) has been an area of continued growth for the damage assessment of materials. The need for NDT/E methods has increased dramatically in recent years due to the high demand from end-users for[1]: product safety, in-line diagnostics, quality control, health monitoring and secure testing. Moreover, due to the high cost of inspection in both metallic and composite materials, development of reliable and effective NDT/E methods to detect the occurrence of critical failure modes has been pursued[2-5]. For this scope, numerous ultrasonic inspection techniques have been developed over the past twenty years to detect and localise material defects such as micro-cracks, delamination and weak adhesive bonds[6-8].

Early work, focusing on single frequency excitation, by Breazeale and Thompson [9], Suzuki, et al. [10] and Gauster and Breazeale [11] relate the production of higher order harmonics to the deviation of Hooke's law in a nonlinear medium, which forms the foundation for damage detection using nonlinear ultrasound methods. After which the development of dual frequency (modulation) nonlinear ultrasound excitation methods have been demonstrated experimentally by multiple authors [12-15]. It is a well-known issue, that large ultrasonic wave excitation amplitudes of mediums are required in order to produce observable nonlinearities, which can be up to three orders of magnitude (or more) smaller than the fundamental response. Thus, by improving the signal to noise ratios of damage/defect produced harmonics or enhancing their response by efficient signal processing methods there can be improvements in harmonic detection as well as the quantification of damage/defects.

In damaged media such as aluminium, steel, composite laminates and numerous others, the nonlinear interaction of elastic waves with the structural defect can be mathematically treated as an expansion of the elastic energy as a power series with

respect to the strain[16]. As a result of this nonlinear interaction, harmonics (i.e. both even and odd multiples) and sub-harmonics (sub-multiples) of the single periodic transmitted signal can be generated, with the contribution of the second harmonic wave dominant with respect to others. Hence, second harmonic is traditionally used to indicate the presence of structural defects within the material. Both experimental and numerical evidence[17-21] has shown that these nonlinear elastic effects are caused by the clapping and rubbing motion of damage surfaces, i.e. when the micro-crack is subject to either tensile/compression or shear stresses at its contact interfaces.

Similarly, modulated nonlinear waves (sidebands) with dual harmonic excitation have revealed higher sensitivity to micro-damage[22]. The main benefit of dual harmonic transmission is that equipment-based nonlinearities, which are often generated in single periodic excitation are not present. Hence, the generation of nonlinear modulation effects can unequivocally be related to the material response without the need of advanced signal processing tools[23,24]. However, although significant progress has been made with regard to nonlinear modulation methods, full-scale implementation has been limited by the relative low signal-to-noise-ratio (SNR) of nonlinear modulated waves in the measured Fourier spectrum.

Many signal processing methods have been developed for the processing of ultrasound responses which broadly form two functions, either filtering or amplification of signal responses. Specifically, within the nonlinear ultrasound field methods such as Hilbert-Huang transforms[25], wavelet analysis[26], scaling subtraction[27] and sideband imaging[28] have all been used to improve damage/defect detection.

The Hilbert-Huang transform was used to demodulate nonlinear signals into the instantaneous frequency and amplitude, where damage is then based on these instantaneous characteristics. Wavelet analysis allows for the evaluation of signals in

both time and frequency while providing high resolution in both, which allow for improved accuracy when determining ultrasonic signal arrival times leading to enhanced impact localisation. The scaling subtraction method relies on the scaling of a linear ultrasound signal to a nonlinear signal and the subsequent subtraction of the two signals, leaving only the nonlinear component after subtraction. While these methods provide improvement in the detection and analysis of nonlinear modulated signals, they do not provide solutions for evaluating modulation when sidebands fall below the noise level of the captured response.

This paper addresses the problem of enhancing the detection of sidebands and, therefore, improving the efficiency of the nonlinear modulation techniques, by focusing on the symmetry (or invariance) properties of ultrasonic phenomena in damage materials with micro-cracks. The analysis of invariants properties of nonlinear systems has been investigated in many fields of science. For example, symmetry properties associated with the infinitesimals of Lie groups have been used to determine the motion of particles propagating in a medium with non-classical nonlinearity[29].

This research work presents a new signal processing technique under the framework of phase symmetry analysis (PSA)[30,31] for the filtering of sidebands without altering measured ultrasonic signals. PSA, in particular, exploits the invariant properties of damaged materials by shifting the phase angle, ϕ, of both single and dual periodic input signals to enhance the detection of nonlinear elastic waves. The proposed technique allows, for the first time, determining the phase angle of dual input waveforms in order to extract only sidebands and filter out other frequency components contained in the measured spectrum. It is important to note, that under single frequency PSA, a doubling of the second harmonic response is expected, while considering modulation a tripling of the response is expected. The doubling and tripling effect of PSA is important, with

regard to improving SNRs and is one of the main benefits along with the simplicity of this type of signal processing method. Theoretically, sidebands which are greater than a 1/3rd of the noise level can be measured, resulting in improved sensitivity in the discovery and evaluation of damage/defects.

This signal processing technique was experimentally validated on a fatigued isotropic metallic structure with micro-cracks and a carbon fibre reinforced plastic (CFRP) composite sample with internal delamination. These two damage types were chosen specifically for their high occurrence, but also as they both lead to catastrophic failure of components or structures found in a wide range of engineering disciplines (civil, aerospace and oil and gas). Fatigue cracks in metallic structures are by far the most common failure mechanism, with obvious issues relating to discovery and evaluation. Composite components are sensitive to low velocity impact damage that can considerably degrade the structural integrity and, if not detected, result in catastrophic failures[32,33]. The layout of the paper is as follows: Section 2 provides information about the experimental set-up for the PSA experiments. Sections 3 and 4 illustrates the theory of PSA for both single and dual excitation to filter out second harmonic and sideband waves, respectively. Section 5 reports the NEWS experimental results with PSA analysis. Conclusions are provided at the end of the paper.

2. Equipment Set-up

The proposed PSA methodology was tested on an aluminum fatigue sample and a flat composite panel undergone to impact damage. The CFRP sample has width of 250 mm, length of 350 mm and thickness of 13 mm. Considering a coordinate system starting at the bottom left of the CFRP plate (0,0), the impact location is located at (130,190). One of the main features of nonlinear ultrasound testing techniques is that they do not

require prior information of the mechanical properties of the test specimen, thus the composite stacking sequence and impact energy are unknown. An aluminium plate (AA2024) specifically designed according to ASTM standards for fatigue crack growth [Figure 1 (a)] was used. The fatigue coupon had a length of 185 mm, width of 50 mm and thickness of 8 mm. A 2.4 mm notch was machined and then tapered in from both edges to a fine point, with a total depth of 8 mm. The fatigue crack was induced through a fatigue machine (Instron 8801), which allowed the plate to be fixed with hydraulic clamps and apply low-cycle fatigue loading until a significant fatigue crack had propagated (length 13.07 mm, measured with an optic microscope Leyca M205 C). For the aluminium sample, the excitation transducers (Tx) were located 30 mm to the left of the centre of the notch and 20 mm (Tx 1) and 35 mm (Tx 2) down, with the receiving transducer (Rx) located 30 mm to the right of the centre of the notch and 27 mm down [Figure 1 (a)]. For the composite sample Tx 1 and Tx 2 were located 30 mm away from the centre of the impact zone [Figure 1 (b) and (c)] and 185 mm and 215 mm down, respectively. Rx 1 was located 30 mm to the right of the centre of the impact zone and 200 mm down [Figure 1 (b)].

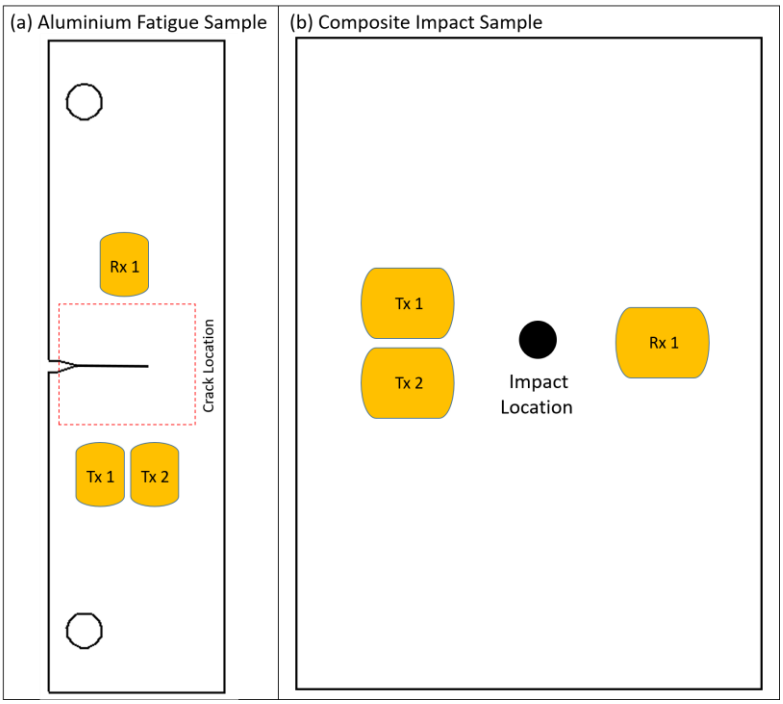

Figure 1: Aluminium Fatigue sample (a) and impacted composite sample (b)

Table 1 shows the excitation procedure for each sample and transducer location Tx 1 and Tx 2. Both single frequency excitation and the proposed PSA method with dual driving frequencies were evaluated. A sweep between 100 kHz and 300 kHz was conducted on each sample, with the highest peak of the captured FFT used for the single frequency excitation and the highest two chosen as the two modulation signals.

Table 1: Excitation procedure for modulation and PSA testing.

Sample	**Tx 1 (f_p)**	**Tx 2 (f_q)**	$2f_p$	$f_p - f_q$	$f_p + f_q$
Aluminium (single frequency)	116 kHz		232 kHz		
Aluminium (dual frequency)	116 kHz	250 kHz	232 kHz	134 kHz	366 kHz
Composite (dual frequency)	101.5 kHz	150.5 kHz	203 kHz	49 kHz	252 kHz

A continuous signal was used to excite the aluminium and composite samples from locations Tx 1 (116 kHz) and Tx 2 (232 kHz) at an output of 80 Vpp. A single frequency excitation method was also conducted for the aluminium sample from Tx 1 (116 kHz) and captured at Rx 1 (see Table 1). In order to evaluate the effects of the excitation amplitude on the production of sidebands the composite sample tests were conducted at multiple voltages (5 V, 20 V, 40 V, 60 V and 80 V). Nonlinearities are only generated once a minimum energy threshold is applied to the damage region, thus generally high voltage (high energy) excitation of the structure is required. Measurements for the aluminium and composite plates were captured with a sampling frequency of 2 MHz at the Rx 1 location. The Tx signals were generated using a function generator (TTI 50 MHz Pulse Generator T6501) linked to an amplifier (Falco Systems DC 5 MHz High Voltage WMA-300), and applied to the structure with a piezoelectric active transducer (McWade Acoustic Emission Sensor Type NS3303 with width of 2 cm, length of 2.3 cm and thickness of 1 cm) with a resonance frequency of 150 kHz. The table below shows the relative phase of the Tx signals (determined in theory section below) that are needed to isolate each of the sidebands. Three signals were sent from Tx 1 and Tx 2 at a phase of 0°, 120°,240° for both in order to isolate the $f_p + f_q$ modulation component, and 0°(0°), 120°(-120°),240°(-240°) for Tx 1(Tx 2) for $f_p - f_q$.

Table 2: Phase of Tx signals for PSA testing.

Sideband Component	**Tx 1 (f_p) Phase angle(ϕ)**	**Tx 2 (f_q) Phase angle(ϕ)**
$f_p + f_q$	0°, 120°,240°	0°, 120°,240°
$f_p - f_q$	0°, 120°,240°	0°, -120°,-240°

3. Theory of PSA with Single Harmonic Excitation

The basic concept of PSA with single excitation (also known in literature as “pulse compression”) is first introduced in order to extract the nonlinear second harmonic

response in damaged materials. This model is then extended to dual excitation (see Section 4) as for the novelty of this work.

3.1. Continuous Excitation

In order to perform PSA with phase shifted driving signals, let us consider first a periodic input signal, $x(t) = A\cos(2\pi ft + \phi)$, with A the amplitude, f the input frequency and ϕ the phase. Assuming that the nonlinear behaviour of the medium is described through a second order nonlinear system, the output $y(t)$ received by the receiver transducer can be expressed through a Volterra functional series as follows[34]:

$$\begin{aligned} y(t) &= \sum_{n=1}^{3} y_n(t) = y_1(t) + y_2(t) + \cdots \\ &= \int_{-\infty}^{+\infty} h_1(\tau_1) x(t-\tau_1) d\tau_1 \\ &+ \int_{-\infty}^{+\infty} d\tau_1 \int_{-\infty}^{+\infty} h_2(\tau_1, \tau_2) x(t-\tau_1) x(t-\tau_2) d\tau_2 \end{aligned} \quad (1.1)$$

where $y_1(t)$ and $y_2(t)$ are the system partial responses of the linear and second order, respectively. The nth order kernel of Eq. (1.1), $h_n(\tau_1,\ldots,\tau_n)$, is called the *nonlinear impulse response* of order n. This term includes all the nonlinear propagation effects through the medium. Its Fourier transform is called the *nonlinear transfer function* of order n:

$$H_n(f_1,\ldots,f_n) = \frac{1}{(2\pi)^n} \int_{-\infty}^{+\infty} \cdots \int_{-\infty}^{+\infty} h_n(\tau_1,\ldots,\tau_n) e^{-j[2\pi(f_1\tau_1+\cdots+f_n\tau_n)]} d\tau_1 \cdots d\tau_n . \quad (1.2)$$

Since $h_n(\tau_1,\ldots,\tau_n)$ is a symmetric function of the arguments $(\tau_1,\ldots,\tau_n)$, it follows that $H_n(f_1,\ldots,f_n)$ is symmetric for $(f_1,\ldots,f_n)$. In addition, from the above equation, it can be noted that the usual properties of spectral conjugation still hold:

$$H_n^*(f,\ldots,f_n) = H_n(-f_1,\ldots,-f_n). \quad (1.3)$$

Hence, solving the multiple integrals of Eq. (1.1), the following terms are obtained[35]:

Linear Term:

$$y_1(t) = \int_{-\infty}^{+\infty} h_1(\tau_1) x(t-\tau_1) d\tau_1 = \frac{A}{2} H_1(f) e^{j(2\pi ft+\phi)} + \text{conjugate term} \qquad (1.4)$$

with $H_1(f) = \frac{1}{2\pi} \int_{-\infty}^{+\infty} h_1(\tau_1) e^{-j2\pi f\tau_1} d\tau_1$.

Second Order Term:

$$\begin{aligned} y_2(t) &= \int_{-\infty-\infty}^{+\infty+\infty} h_2(\tau_1,\tau_2) x(t-\tau_1) x(t-\tau_2) d\tau_1 d\tau_2 \\ &= \frac{A^2}{4} H_2(f,f) e^{j(4\pi ft+\phi)} + \text{dc term} + \text{conjugate terms} \end{aligned} \qquad (1.5)$$

with $H_2(\omega,\omega) = \frac{1}{(2\pi)^2} \int_{-\infty-\infty}^{+\infty+\infty} h_2(\tau_1,\tau_2) e^{-j2\pi f\tau_1} e^{-j2\pi f\tau_2} d\tau_1 d\tau_2$.

Hence, neglecting dc terms unrelated to the phase of the signal and the conjugate terms in Eqs. (1.4) and (1.5), Eq. (1.1) becomes:

$$y(t) = \frac{A}{2}\left[H_1(f) e^{j(2\pi ft+\phi)} + \frac{A}{2} H_2(f,f) e^{j[2(2\pi ft+\phi)]} \right] \qquad (1.6)$$

Extraction of Second Harmonic

PSA can be used to eliminate the linear contribution from the acquired signals by simply imposing the *second order symmetry condition*, $j\phi = \pm \pi kj$, with $k \in \aleph$, where $\aleph$ is the set of all natural numbers. Such invariant condition is fulfilled for two different phase angles, $\phi = 0$ and $\phi = \pi$. Indeed, PSA consists in sending two phase shifted harmonic waveforms into the damaged structure, in order to extract the second order nonlinear signature:

$$y(t)\big|_{\phi=0} = \frac{A}{2}\left[H_1(f)e^{j2\pi ft} + \frac{A}{2}H_2(f,f)e^{j4\pi ft} \right]$$
$$y(t)\big|_{\phi=\pi} = \frac{A}{2}\left[-H_1(f)e^{j2\pi ft} + \frac{A}{2}H_2(f,f)e^{j4\pi ft} \right] \quad (1.7)$$

Hence, by simply summing the two output signals as in Eq. (1.7), it yields:

$$y_{PSA}(t) = y(t)\big|_{\phi=0} + y(t)\big|_{\phi=\pi} = \frac{1}{2}A^2 H_2(f,f)e^{j4\pi ft} \quad (1.8)$$

Thus, the sum term in Eq. (1.8) corresponds only to the nonlinear second harmonic contribution. The result obtained in Eq. (1.8) is equivalent to a pulse inversion (PI) operation.

3.2. Burst Excitation

In order to perform the second order PSA with phase shifted driving signals, a single tone burst solution for $x(t)$ with a limited number of cycles can be used. Such an input waveform allows a clear differentiation of the starting and ending points from the background noise. A high number of cycles enables the tone burst to resemble a continuous signal [see Figure 2 (a)]. Indeed, the spectrum $X(\omega)$ of a tone burst for a central angular frequency $\omega = 2\pi f$ is:

$$X(\omega) = \mathrm{a}\cos(\omega t) \quad (1.9)$$

where *a* is the input amplitude that can be expressed as:

$$a = A\frac{N}{N+M}\left(\frac{\sin q}{q} \mp \frac{\sin r}{r} \right) \quad (1.10)$$

where *N* is the number of cycles of the tone-burst, *M* is the number of cycles between two consecutive bursts, whilst q and r are defined as $q = N[1/(N+M)-1]\pi$ and $r = N[1/(N+M)+1]\pi$, respectively. The tone burst spectrum envelope is centred on the central frequency *f* of the cosine function. The bandwidth of the fundamental peak [Figure 2 (b)] depends on the number of cycles *N* through the ratio. In this work, the

number of cycles *N* was increase up to 200 cycles, so that the spectrum approaches the case of a continuous waveform.

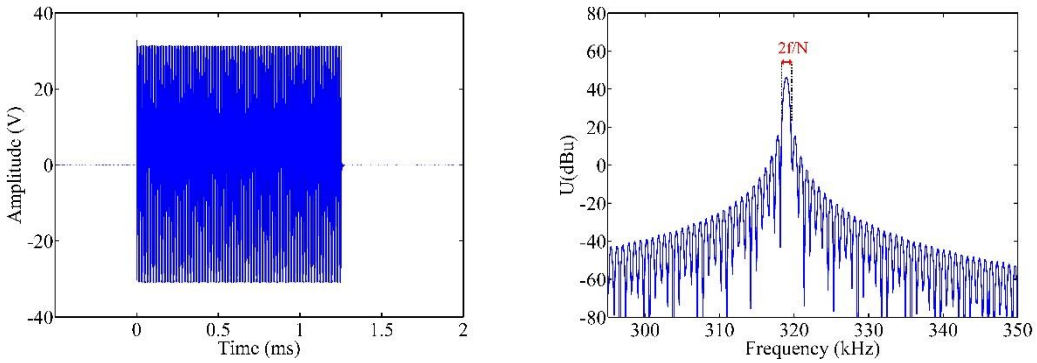

(a) (b)

Figure 2: (a) N = *200* cycle burst time domain, (b) N = *200* cycle burst spectrum.

4. PSA with Dual Harmonic Excitation

Considering now the case of dual (or bi-harmonic) excitation, $x(t) = A\cos(\omega_p t + \phi_p) + B\cos(\omega_q t + \phi_q)$, with $p \neq q$, A and B the amplitudes of the two harmonic inputs, f_p and f_q the input frequencies, with $f_p > f_q$, and ϕ_p and ϕ_q the associated phases. In order to analyse only the sidebands contribution $f_p + f_q$ and $f_p - f_q$ in the measured modulation signal, the nonlinear behaviour of the medium is described through a second order nonlinear system. Thereby, similarly to the case of single harmonic excitation, the output $y(t)$ measured by the receiver transducer can be expressed by a second order Volterra series. Hence, substituting the dual harmonic excitation in Eq. (1.1) we obtain:

Linear Term:

$$
\begin{aligned}
y_1(t) &= \int_{-\infty}^{+\infty} h_1(\tau_1)x(t-\tau_1)d\tau_1 \\
&= \frac{A}{2}H_1(f_p)e^{j(2\pi f_p t+\phi_p)} + \frac{B}{2}H_1(f_q)e^{j(2\pi f_q t+\phi_q)} + \text{conjugate terms}
\end{aligned}
\tag{1.11}
$$

with $H_1(f_p) = \frac{1}{2\pi}\int_{-\infty}^{+\infty} h_1(\tau_1)e^{-j2\pi f_p\tau_1}d\tau_1$ and $H_1(f_q) = \frac{1}{2\pi}\int_{-\infty}^{+\infty} h_1(\tau_1)e^{-j2\pi f_q\tau_1}d\tau_1$.

Second Order Term:

$$
\begin{aligned}
y_2(t) &= \int_{-\infty-\infty}^{+\infty+\infty} h_2(\tau_1,\tau_2)x(t-\tau_1)x(t-\tau_2)d\tau_1 d\tau_2 \\
&= \frac{A^2}{4}H_2(f_p, f_p)e^{j4\pi f_p t}e^{j2\phi_p} + \frac{AB}{2}H_2(f_p, f_q)e^{j[2\pi(f_p+f_q)t]}e^{j(\phi_p+\phi_q)} \\
&+ \frac{AB}{2}H_2(f_p,-f_q)e^{j[2\pi(f_p-f_q)t]}e^{j(\phi_p-\phi_q)} + \frac{B^2}{4}H_2(f_q, f_q)e^{j4\pi f_q t}e^{j2\phi_q} \\
&+ \text{dc terms} + \text{conjugate terms}
\end{aligned}
\tag{1.12}
$$

with

$$H_2(f_p, f_p) = \frac{1}{(2\pi)^2}\int_{-\infty-\infty}^{+\infty+\infty} h_2(\tau_1,\tau_2)e^{-j2\pi f_p\tau_1}e^{-j2\pi f_p\tau_2}d\tau_1 d\tau_2,$$

$$H_2(f_p, f_q) = \frac{1}{(2\pi)^2}\int_{-\infty-\infty}^{+\infty+\infty} h_2(\tau_1,\tau_2)e^{-j2\pi f_p\tau_1}e^{-j2\pi f_q\tau_2}d\tau_1 d\tau_2,$$

$$H_2(f_p,-f_q) = \frac{1}{(2\pi)^2}\int_{-\infty-\infty}^{+\infty+\infty} h_2(\tau_1,\tau_2)e^{-j2\pi f_p\tau_1}e^{j2\pi f_q\tau_2}d\tau_1 d\tau_2 \quad \text{and}$$

$$H_2(f_q, f_q) = \frac{1}{(2\pi)^2}\int_{-\infty-\infty}^{+\infty+\infty} h_2(\tau_1,\tau_2)e^{-j2\pi f_q\tau_1}e^{-j2\pi f_q\tau_2}d\tau_1 d\tau_2$$

Neglecting dc and conjugate terms in Eq. (1.11) and (1.12), Eq. (1.1) becomes:

$$
\begin{aligned}
y(t) &= \frac{A}{2}\left[H_1(f_p)e^{j(2\pi f_p t+\phi_p)} + \frac{A}{2}H_2(f_p, f_p)e^{j[2(2\pi f_p t+\phi_p)]} + BH_2(f_p, f_q)e^{j[2\pi(f_p+f_q)t+(\phi_p+\phi_q)]}\right] \\
&+ \frac{B}{2}\left[H_1(f_q)e^{j(2\pi f_q t+\phi_q)} + \frac{B}{2}H_2(f_q, f_q)e^{j[2(2\pi f_q t+\phi_q)]} + AH_2(f_p,-f_q)e^{j[2\pi(f_p-f_q)t+(\phi_p-\phi_q)]}\right]
\end{aligned}
$$

(1.13)

Extraction of $\mathbf{f}_+ = \mathbf{f}_p + \mathbf{f}_q$

In order to extract only the sideband $f_+ = f_p + f_q$ from the measured signal, let us impose the symmetry condition $j(\phi_p + \phi_q) = \pm j2\pi k$, so that $\phi_p = -\phi_q$. Therefore, Eq. (1.13) becomes:

$$y(t) = \frac{A}{2}\left[H_1(f_p) e^{j(2\pi f_p t + \phi_p)} + \frac{A}{2} H_2(f_p, f_p) e^{j[2(2\pi f_p t + \phi_p)]} + BH_2(f_p, f_q) e^{j[2\pi(f_p + f_q)t]} \right]$$
$$+ \frac{B}{2}\left[H_1(f_q) e^{j(2\pi f_q t - \phi_p)} + \frac{B}{2} H_2(f_q, f_q) e^{j[2(2\pi f_q t - \phi_p)]} + AH_2(f_p, -f_q) e^{j[2\pi(f_p - f_q)t + 2\phi_p]} \right]$$

(1.14)

To eliminate other contributions, we pose $\phi_p = 0$, $\phi_p = 2/3\pi$ and $\phi_p = -2/3\pi$ so that:

$$y(t)\Big|_{\phi_p = 0} = \frac{A}{2}\left[H_1(f_p) e^{j2\pi f_p t} + \frac{A}{2} H_2(f_p, f_p) e^{j4\pi f_p t} + BH_2(f_p, f_q) e^{j[2\pi(f_p + f_q)t]} \right],$$
$$+ \frac{B}{2}\left[H_1(f_q) e^{j2\pi f_q t} + \frac{B}{2} H_2(f_q, f_q) e^{j4\pi f_q t} + AH_2(f_p, -f_q) e^{j[2\pi(f_p - f_q)t]} \right]$$

(1.15)

$$y(t)\Big|_{\phi_p = \frac{2}{3}\pi} = \frac{A}{4}\left[-H_1(f_p) e^{j2\pi f_p t} - \frac{A}{2} H_2(f_p, f_p) e^{j4\pi f_p t} + 2BH_2(f_p, f_q) e^{j[2\pi(f_p + f_q)t]} \right]$$
$$- \frac{B}{4}\left[H_1(f_q) e^{j2\pi f_q t} + \frac{B}{2} H_2(f_q, f_q) e^{j4\pi f_q t} + AH_2(f_p, -f_q) e^{j[2\pi(f_p - f_q)t]} \right]$$

(1.16)

and

$$y(t)\Big|_{\phi_p = -\frac{2}{3}\pi} = \frac{A}{4}\left[-H_1(f_p) e^{j2\pi f_p t} - \frac{A}{2} H_2(f_p, f_p) e^{j4\pi f_p t} + 2BH_2(f_p, f_q) e^{\left[j2\pi(f_p + f_q)t\right]} \right]$$
$$- \frac{B}{4}\left[H_1(f_q) e^{j2\pi f_q t} + \frac{B}{2} H_2(f_q, f_q) e^{j4\pi f_q t} + AH_2(f_p, -f_q) e^{j[2\pi(f_p - f_q)t]} \right]$$

(1.17)

Hence:

$$y_{PSA}(t) = y(t)\Big|_{\phi_p = 0} + y(t)\Big|_{\phi_p = \frac{2}{3}\pi} + y(t)\Big|_{\phi_p = -\frac{2}{3}\pi} = \frac{3}{2} ABH_2(f_p, f_q) e^{j[2\pi(f_p + f_q)t]} \qquad (1.18)$$

Extraction of $\mathbf{f}_{-} = \mathbf{f}_p - \mathbf{f}_q$

In order to extract only the sideband $f_{-} = f_p - f_q$ from the measured signal, let us impose the symmetry condition $j(\phi_p - \phi_q) = \pm j2\pi k$, so that $\phi_p = \phi_q$. Therefore, Eq. (1.13) becomes:

$$y(t) = \frac{A}{2}\left[H_1(f_p) e^{j(2\pi f_p t + \phi_p)} + \frac{A}{2} H_2(f_p, f_p) e^{j[2(2\pi f_p t + \phi_p)]} + BH_2(f_p, f_q) e^{j[2\pi(f_p + f_q)t + 2\phi_p]} \right]$$
$$+ \frac{B}{2}\left[H_1(f_q) e^{j(2\pi f_q t + \phi_p)} + \frac{B}{2} H_2(f_q, f_q) e^{j[2(2\pi f_q t + \phi_p)]} + AH_2(f_p, -f_q) e^{j[2\pi(f_p - f_q)t]} \right]$$

(1.19)

To eliminate other contributions: $\phi_p = 0$, $\phi_p = 2/3\pi$ and $\phi_p = -2/3\pi$ so that:

$$y(t)\Big|_{\phi_p = 0} = \frac{A}{2}\left[H_1(f_1) e^{j2\pi f_p t} + \frac{A}{2} H_2(f_p, f_p) e^{j4\pi f_p t} + BH_2(f_p, f_q) e^{j[2\pi(f_p + f_q)t]} \right]$$
$$+ \frac{B}{2}\left[H_1(f_q) e^{j2\pi f_q t} + \frac{B}{2} H_2(f_q, f_q) e^{j4\pi f_q t} + AH_2(f_p, -f_q) e^{j[2\pi(f_p - f_q)t]} \right],$$

(1.20)

$$y(t)\Big|_{\phi_p = \frac{2}{3}\pi} = -\frac{A}{4}\left[H_1(f_p) e^{j2\pi f_p t} + \frac{A}{2} H_2(f_p, f_p) e^{j4\pi f_p t} + BH_2(f_p, f_q) e^{j[2\pi(f_p + f_q)t]} \right]$$
$$+ \frac{B}{4}\left[-H_1(f_q) e^{j2\pi f_q t} - \frac{B}{2} H_2(f_q, f_q) e^{j4\pi f_q t} + 2AH_2(f_p, -f_q) e^{j[2\pi(f_p - f_q)t]} \right]$$

(1.21)

and

$$y(t)\Big|_{\phi_p = -\frac{2}{3}\pi} = -\frac{A}{4}\left[+H_1(f_p) e^{j2\pi f_p t} + \frac{A}{2} H_2(f_p, f_p) e^{j4\pi f_p t} + BH_2(f_p, f_q) e^{j[2\pi(f_p + f_q)t]} \right]$$
$$+ \frac{B}{4}\left[-H_1(f_q) e^{j2\pi f_q t} - \frac{B}{2} H_2(f_q, f_q) e^{j4\pi f_q t} + 2AH_2(f_p, -f_q) e^{j[2\pi(f_p - f_q)t]} \right]$$

(1.22)

Hence:

$$y_{PSA}(t) = y(t)\big|_{\phi_p=0} + y(t)\big|_{\phi_p=\frac{2}{3}\pi} + y(t)\big|_{\phi_p=-\frac{2}{3}\pi} = \frac{3AB}{2} H_2(f_p, -f_q) e^{j[2\pi(f_p - f_q)t]}$$

(1.23)

5. Discussion and Results.

5.1. Single frequency results: Aluminum

Figure 3 illustrates the spectrum measured by a receiver transducer surface bonded on a damaged aluminium plate containing both the fundamental and the second harmonic. The driving frequency was f = 116 kHz, so that the second harmonic is at $2f$ = 232 kHz.

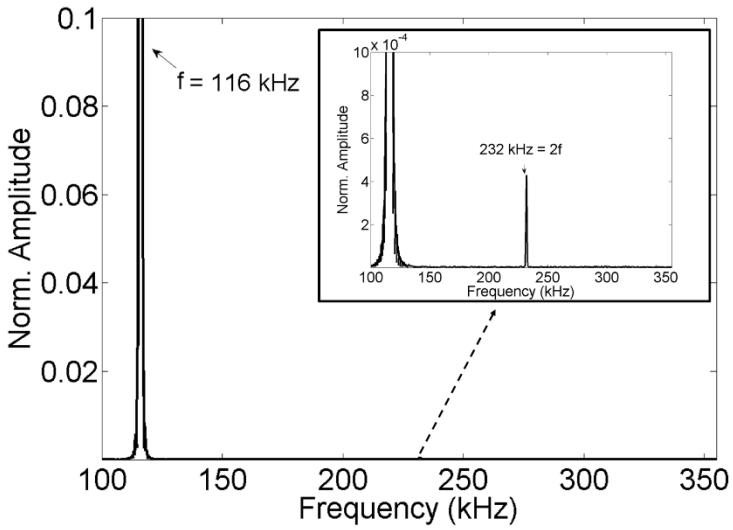

Figure 3: Ultrasonic spectrum measured on a damaged aluminium plate using a single harmonic input f = 116 kHz.

Figure 4 (a) illustrates the time histories of the two input signal opposite in phase represented by a continuous black and a dashed red line, as well as the output signal obtained after PSA (green line). Figure 4 (b) shows the signal spectrum after PSA. It can be clearly seen that whilst the linear contribution is eliminated in the output signal, the amplitude of the second order nonlinear contribution at $2f$ = 232 kHz is almost doubled.

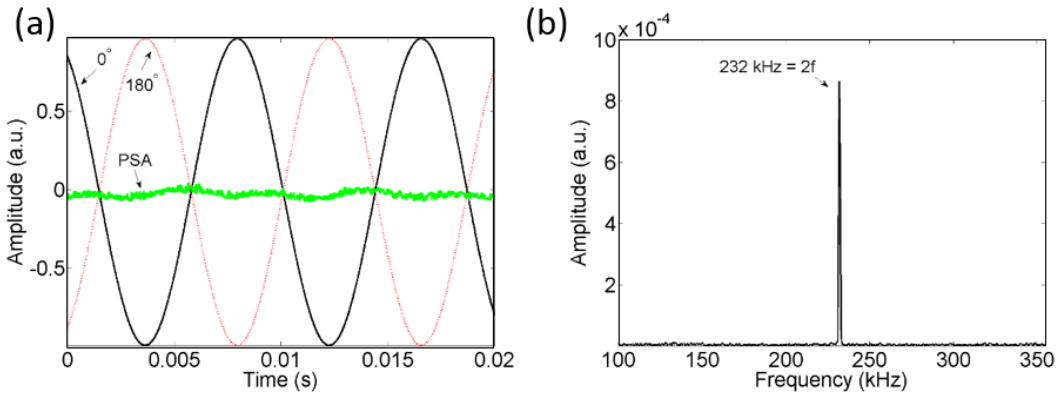

Figure 4: Time history of the two input harmonic waveforms and the signal after PSA (a), and the associated spectrum after PSA (b).

5.2. Dual Frequency Results: Aluminum Sample

Figure 5 illustrates the spectrum measured by a receiver transducer (surface bonded) on the same damaged aluminium plate containing the modulated frequencies (sidebands). The two harmonic input were f_p = 250 kHz and f_q = 116 kHz, so that the two sidebands frequencies were f_- = 134 kHz and f_+ = 366 kHz. Note that also the second harmonic frequency of f_q is contained in the signal's spectrum (i.e. $2f_q$ = 232 kHz).

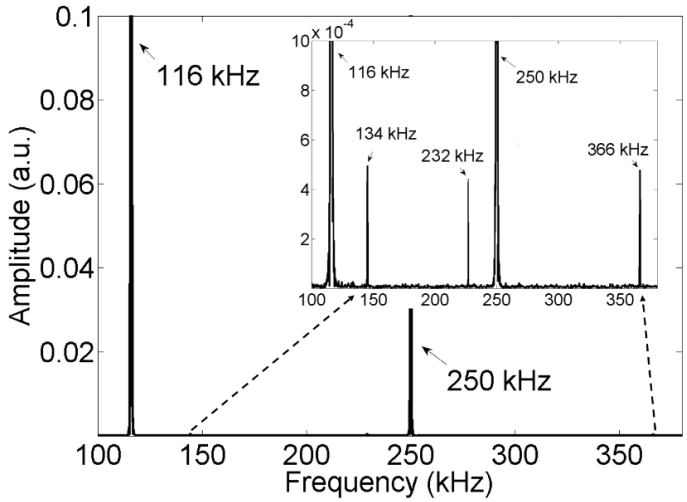

Figure 5: Ultrasonic spectrum measured on a damaged aluminium plate using two excitation frequencies were f_p = 250 kHz and f_q = 116 kHz.

Figure 6 (a) illustrates the time histories of the three input signal at different phases (i.e. 0°, 120° and 240°) and the output signal obtained after PSA (green line). Figure 6 (b)

shows the signal spectrum after PSA. Whilst both linear and second order nonlinear contributions are eliminated in the output signal, the amplitude of the sideband f_+ = 366 kHz is almost tripled. Figure 6 (c) shows the signal spectrum after PSA. It can be clearly seen that whilst both linear and second order nonlinear contributions are eliminated in the output signal, the amplitude of the sideband f_- = 134 kHz is almost tripled.

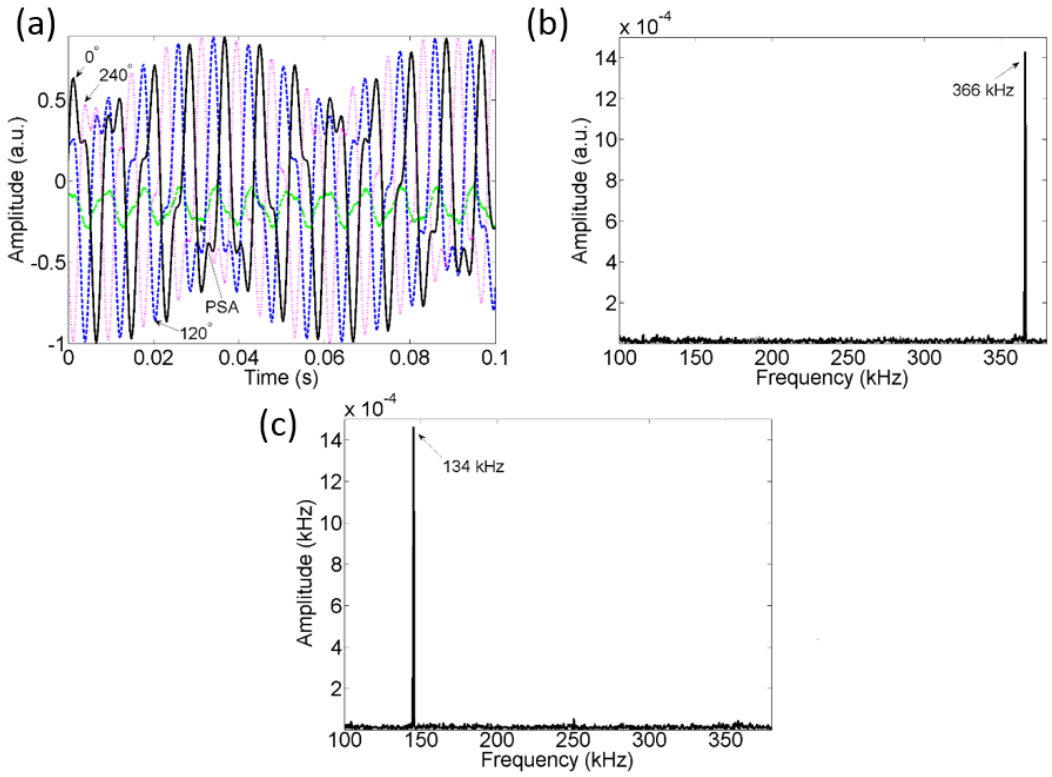

Figure 6: Time history of the three input harmonic waveforms and the signal after PSA (a), and the associated spectrum after PSA showing the sideband $f_+ = f_p + f_q$ (b), $f_- = f_p - f_q$ (c).

5.3. Dual Frequency Results: Composite Plate

Figure 7 illustrates the spectrum measured by a receiver transducer surface bonded on the damaged composite plate containing the modulated frequencies (sidebands). The two harmonic input were f_p = 101.5 kHz and f_q = 150.5 kHz, so that the two sidebands

frequencies were f_- = 49 kHz and f_+ = 252 kHz. Note that also the second harmonic frequency of f_p is contained in the signal spectrum (i.e. $2f_q$ = 203 kHz).

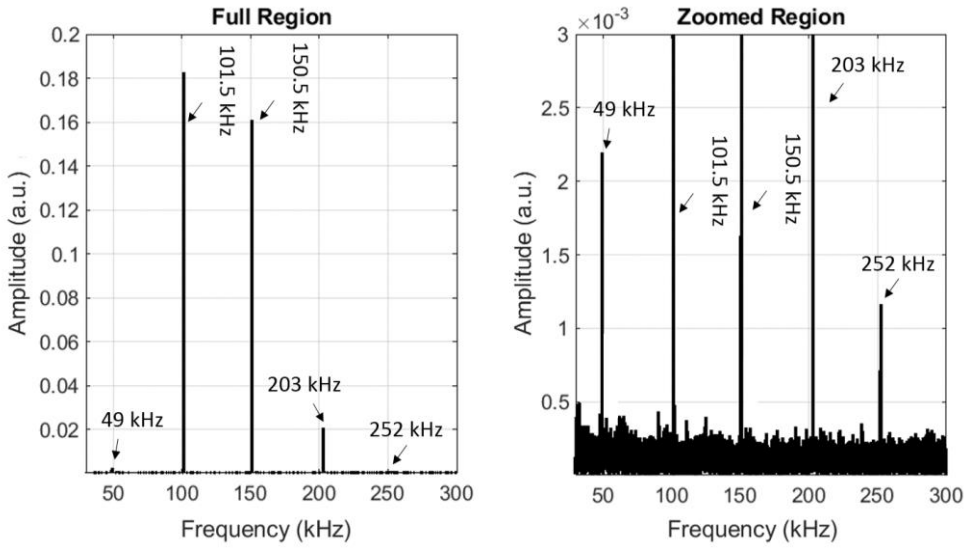

Figure 7: Composite samples signal spectrum before PSA showing multiple sidebands.

In order to evaluate the generation and capability of the PSA method to improve sideband visibility, multiple excitation voltages were used to determine sideband amplitude as excitation voltage increased. Five excitation voltage levels were evaluated: 5 V, 20 V, 40 V, 60 V and 80 V. Figure 8 shows the response after PSA for 40 V, 60 V and 80 V. No sideband responses were visible up to and including 40V, this is clear in Figure 8 (a) and (b) (red dotted line highlights frequency where sidebands should be). Figure 8 (c) to (f) show how the sidebands become visible after a threshold voltage level is achieved, between 40V and 60V. The amplitude of each of sidebands (at 49 kHz and 252 kHz) are sensitive to the discontinuities of the damage region and thus generally not equal in amplitude. In this case the sum frequency at 252 kHz [Figure 8 (d) and (f)] is much greater than at the difference frequency at 49 kHz [Figure 8 (c)

and (e)]. For both frequencies it is clear that the nonlinearity increases as voltage increases.

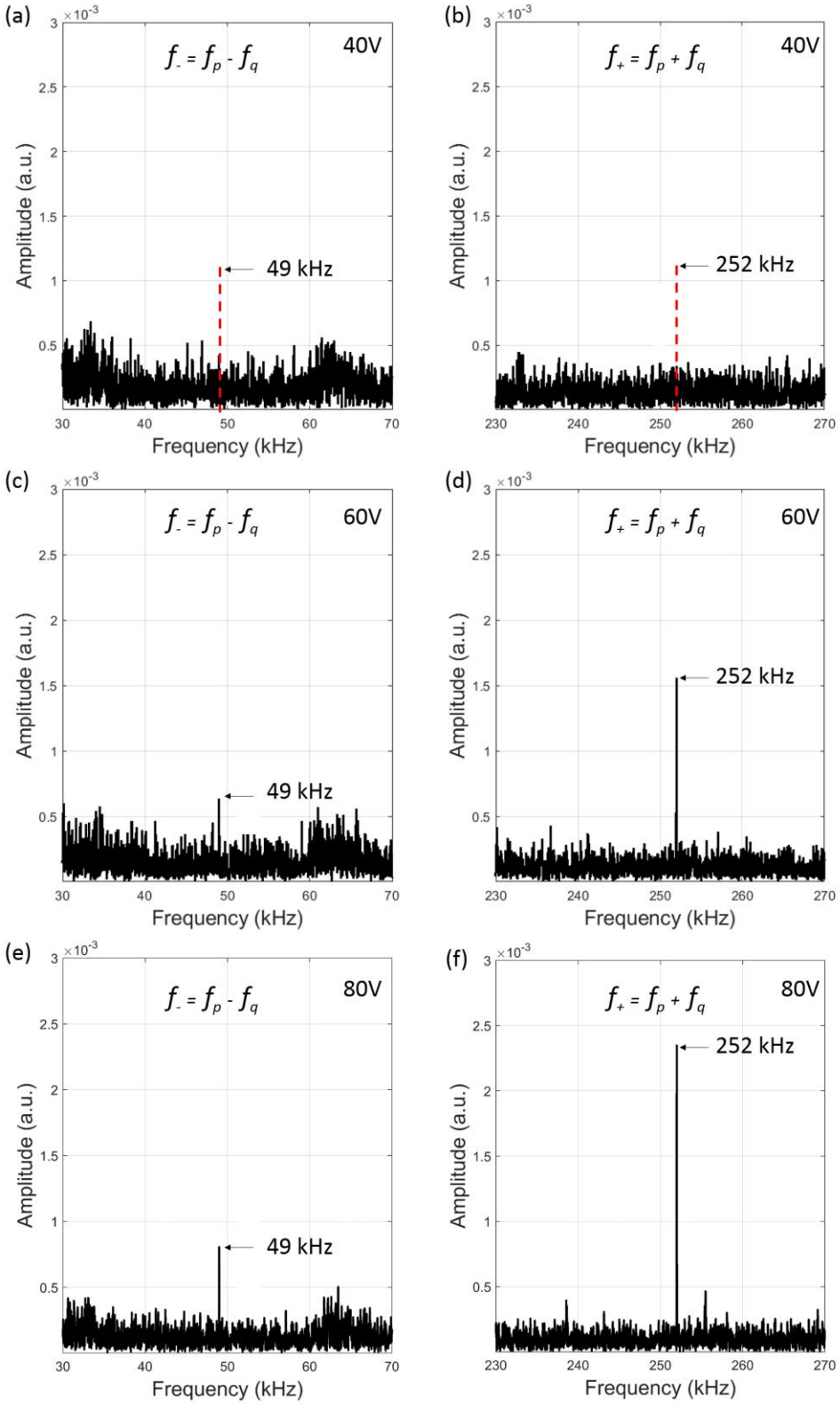

Figure 8: Signal spectrum after PSA showing multiple sidebands as function of the input voltage.

6. Conclusion

This paper has theoretically and experimentally showed that PSA provides an efficient and easy-to-implement solution to the problem of extracting nonlinear sidebands with dual frequency excitation. The proposed methodology was used to characterise modulated sidebands in both metallic and CFRP composite samples by exploiting invariant properties of the phase angle ϕ of excitation signals. Experimental results showed that there is a clear increase in the modulated nonlinear elastic response and a reduction in the linear response after PSA, as well as a decrease in undesired harmonics generation. The increase in the modulated responses were shown to closely follow theoretical predications. For example, considering the single frequency system the second harmonic response (f_1) was doubled, while the modulated responses (f_2+f_1 and f_2-f_1) were tripled, as predicted theoretically. Results presented here can be applied to enhance the extraction of low-amplitude nonlinear responses related to material nonlinearity generated by defects in various media, thus improving signal conditioning for nonlinear ultrasound applications.

REFERENCES

1. C Chen, *Ultrasonic and advanced methods for nondestructive testing and material characterization*. (World Scientific Pub Co Inc, 2007).
2. Y Bar-Cohen, In-Service NDE of Aerospace Structures–Emerging Technologies and Challenges at the end of the 2nd Millennium. *NDT. net* (1999); **4(9)** (9) 1.
3. KS Tan, N Guo, BS Wong, and CG Tui, Experimental evaluation of delaminations in composite plates by the use of Lamb waves. *Compos Sci Technol* (1995); **53** (1) 77.
4. M Lemistre, R Gouyon, H Kaczmarek, and D Balageas, presented at the Office National D Etudes Et De Recherches Aerospatiales Onera-Publications-TP, 1999 (unpublished).
5. Wentao Wang, Hui Zhang, Jerome P Lynch, Carlos ES Cesnik, and Hui Li, Experimental and numerical validation of guided wave phased arrays integrated within standard data acquisition systems for structural health monitoring. *Structural Control and Health Monitoring* (2018); **25** (6) e2171.

6. TJ Ulrich, Paul A Johnson, and Robert A Guyer, Interaction dynamics of elastic waves with a complex nonlinear scatterer through the use of a time reversal mirror. *Physical review letters* (2007); **98** (10) 104301.
7. R. A. Guyer and P. A. Johnson, Nonlinear mesoscopic elasticity: Evidence for a new class of materials. *Physics Today* (1999); **52** (4) 30.
8. Eric B Flynn, See Yenn Chong, Gregory J Jarmer, and Jung-Ryul Lee, Structural imaging through local wavenumber estimation of guided waves. *Ndt & E International* (2013); **59** 1.
9. MA Breazeale and DO Thompson, Finite-amplitude ultrasonic waves in aluminum. *Applied Physics Letters* (1963); **3** (5) 77.
10. Tetsuro Suzuki, Akira Hikata, and Charles Elbaum, Anharmonicity due to glide motion of dislocations. *Journal of Applied Physics* (1964); **35** (9) 2761.
11. Wilhelm Belrupt Gauster and MA Breazeale, Ultrasonic measurement of the nonlinearity parameters of copper single crystals. *Physical Review* (1968); **168** (3) 655.
12. AS Korotkov and AM Sutin, Modulation of ultrasound by vibrations in metal constructions with cracks. *Acoustics Letters* (1994); **18** (4) 59.
13. Alexander M Sutin and Dmitri M Donskoy, presented at the Nondestructive Evaluation of Aging Aircraft, Airports, and Aerospace Hardware II, 1998 (unpublished).
14. Vladimir Zaitsev and Paul Sas, Nonlinear response of a weakly damaged metal sample: a dissipative modulation mechanism of vibro-acoustic interaction. *Journal of Vibration and Control* (2000); **6** (6) 803.
15. Gian Piero Malfense Fierro and Michele Meo, Residual fatigue life estimation using a nonlinear ultrasound modulation method. *Smart Materials and Structures* (2015); **24** (2) 025040.
16. LD Landau and EM Lifshitz, (Pergamon, Oxford, UK, 1986).
17. Francesco Ciampa, Ettore Barbieri, and Michele Meo, Modelling of multiscale nonlinear interaction of elastic waves with three-dimensional cracks. *The Journal of the Acoustical Society of America* (2014); **135** (6) 3209.
18. Olivier Bou Matar, Pierre-Yves Guerder, YiFeng Li, Bart Vandewoestyne, and Koen Van Den Abeele, A nodal discontinuous Galerkin finite element method for nonlinear elastic wave propagation. *The Journal of the Acoustical Society of America* (2012); **131** (5) 3650.
19. Ettore Barbieri and Michele Meo, Time reversal DORT method applied to nonlinear elastic wave scattering. *Wave Motion* (2010); **47** (7) 452.
20. Pier Paolo Delsanto and Marco Scalerandi, A spring model for the simulation of the propagation of ultrasonic pulses through imperfect contact interfaces. *The Journal of the Acoustical Society of America* (1998); **104** (5) 2584.
21. Thomas Goursolle, Samuel Callé, Serge Dos Santos, and Olivier Bou Matar, A two-dimensional pseudospectral model for time reversal and nonlinear elastic wave spectroscopy. *The Journal of the Acoustical Society of America* (2007); **122** (6) 3220.
22. KE-A Van Den Abeele, Paul A Johnson, and Alexander Sutin, Nonlinear elastic wave spectroscopy (NEWS) techniques to discern material damage, part I: nonlinear wave modulation spectroscopy (NWMS). *Journal of Research in Nondestructive Evaluation* (2000); **12** (1) 17.
23. Marco Scalerandi, AS Gliozzi, Caterina Letizia Elisabetta Bruno, Davide Masera, and P Bocca, A scaling method to enhance detection of a nonlinear elastic response. *Applied Physics Letters* (2008); **92** (10) 101912.
24. Francesco Ciampa, Akash Mankar, and Andrea Marini, Phononic crystal waveguide transducers for nonlinear elastic wave sensing. *Scientific reports* (2017); **7** (1) 14712.
25. HF Hu, WJ Staszewski, NQ Hu, RB Jenal, and GJ Qin, Crack detection using nonlinear acoustics and piezoceramic transducers—instantaneous amplitude and frequency analysis. *Smart materials and structures* (2010); **19** (6) 065017.
26. Michele Meo, G Zumpano, M Piggott, and G Marengo, Impact identification on a sandwich plate from wave propagation responses. *Composite structures* (2005); **71** (3-4) 302.
27. Maria Cristina Porcu, Lukasz Pieczonka, Andrea Frau, Wieslaw Jerzy Staszewski, and Francesco Aymerich, Assessing the scaling subtraction method for impact damage detection in composite plates. *Journal of Nondestructive Evaluation* (2017); **36** (2) 33.
28. L Pieczonka, L Zietek, A Klepka, WJ Staszewski, F Aymerich, and T Uhl, Damage imaging in composites using nonlinear vibro-acoustic wave modulations. *Structural Control and Health Monitoring* (2018); **25** (2) e2063.
29. S Dos Santos, L Haumesser, EV Meulen, O Bou Matar, and Vitalyi Gusev, presented at the Ultrasonics Symposium, 2004 IEEE, 2004 (unpublished).

30. Serge Dos Santos and Zdenek Prevorovsky, Imaging of human tooth using ultrasound based chirp-coded nonlinear time reversal acoustics. *Ultrasonics* (2011); **51** (6) 667.
31. Francesco Ciampa and Michele Meo, Nonlinear elastic imaging using reciprocal time reversal and third order symmetry analysis. *The Journal of the Acoustical Society of America* (2012); **131** (6) 4316.
32. Francesco Ciampa and Michele Meo, Impact localization on a composite tail rotor blade using an inverse filtering approach. *Journal of Intelligent Material Systems and Structures* (2014); **25** (15) 1950.
33. Jeong-Beom Ihn and Fu-Kuo Chang, Pitch-catch active sensing methods in structural health monitoring for aircraft structures. *Structural Health Monitoring* (2008); **7** (1) 5.
34. Julian J Bussgang, Leonard Ehrman, and James W Graham, Analysis of nonlinear systems with multiple inputs. *Proceedings of the IEEE* (1974); **62** (8) 1088.
35. Francesco Ciampa, Gennaro Scarselli, and Michele Meo, Nonlinear imaging method using second order phase symmetry analysis and inverse filtering. *Journal of Nondestructive Evaluation* (2015); **34** (2) 7.